Hoxa1 and Hoxb1 are required for pharyngeal arch artery development

Marine Roux, Brigitte Laforest, Nathalie Eudes, Nicolas Bertrand, Sonia Stefanovic, Stéphane Zaffran

Hoxa1 and *Hoxb1* are required for pharyngeal arch artery development

Marine Roux [1], Brigitte Laforest [2], Nathalie Eudes, Nicolas Bertrand [3], Sonia Stefanovic, Stéphane Zaffran *

Aix Marseille Univ, INSERM, GMGF, Marseille, France

A B S T R A C T

Hox transcription factors play critical roles during early vertebrate development. Previous studies have revealed an overlapping function of *Hoxa1* and *Hoxb1* during specification of the rhombomeres from which neural crest cells emerge. A recent study on *Hoxa1* mutant mice documented its function during cardiovascular development, however, the role of *Hoxb1* is still unclear. Here we show using single and compound *Hoxa1*;*Hoxb1* mutant embryos that reduction of *Hoxa1* gene dosage in *Hoxb1*-null genetic background is sufficient to result in abnormal pharyngeal aortic arch (PAA) development and subsequently in great artery defects. Endothelial cells in the 4th PAAs of compound mutant differentiate normally whereas vascular smooth muscle cells of the vessels are absent in the defective PAAs. The importance of *Hoxa1* and *Hoxb1*, and their interaction during specification of cardiac NCCs is demonstrated. Together, our data reveal a critical role for anterior *Hox* genes during PAA development, providing new mechanistic insights into the etiology of congenital heart defects.

Keywords:
Hox
Mouse
Neural crest cells
Great arteries
Pharyngeal arch arteries
Congenital heart defects

1. Introduction

Cardiovascular development is a complex and ordered process that is spatially and temporally regulated. This process includes coordinated septation of the outflow tract (OFT) and patterning and remodeling of the pharyngeal arch arteries (PAAs). Hence, any perturbations in this process may result in a spectrum of cardiovascular abnormalities, as reflected by the high incidence of congenital heart diseases observed at birth (1–2% (Hoffman and Kaplan, 2002)). Malformations of the aortic arch, including interrupted aortic arch type-B (IAA-B), are among the most severe forms of CHD. The cause of these cardiovascular defects is often difficult to determine with certainty, nonetheless, studying factors that control cardiovascular development can help to better understand the etiology of these defects.

In mammals, the pharyngeal arches are transient bilateral bulges that develop in the cranial region of the embryo. Each arch has an external layer of ectoderm and an inner layer of endoderm, and in between these are mesenchymal neural crest-derived cells (NCCs) surrounding a mesodermal core. The heart is connected to the bilateral dorsal aorta by PAAs (Graham and Smith, 2001). The most cranial PAAs, which contribute to the vascularization of derivatives of the 1st and 2nd pharyngeal arches, largely regress while the caudal PAAs (3rd, 4th and 6th) are extensively remodeled to form the mature asymmetric aortic arch and great arteries. Involvement of the cardiac NCC, a subgroup of NCCs arising from the post-otic hindbrain, in the development of the PAAs and subsequent great arteries, has been well documented by neural crest ablation experiments in chick (Kirby et al., 1983; Kirby and Waldo, 1995; Porras and Brown, 2008). Cardiac NCCs originate from rhombomeres (r) 6, 7 and 8 and invade the 3rd, 4th and 6th pharyngeal arches to form the vascular smooth muscle layer of the PAA-derived great vessels (see (Kirby, 2007)). Ablation or genetic deletion of the cardiac NCCs results in vascular malformations, including defective OFT septation and abnormal patterning of the aortic arch arteries and great vessels, indicating that NCCs are crucial for normal development of the PAAs (Jain et al., 2011; Jiang et al., 2002; Kirby et al., 1983).

Among a variety of signaling molecules and transcription factors, several *Hox* proteins and co-factors have been described as important for development of the pharyngeal arch arteries. Indeed, *Hox* genes are involved in hindbrain patterning from which NCCs arise. Recently, Makki and Capecchi (2012) showed that *Hoxa1* impacts great artery patterning by controlling the formation of the 4th PAA (Makki and Capecchi, 2012). The use of several markers of the NCCs demonstrated that *Hoxa1* is required to specify NCCs. Interestingly, absence of another *Hox* gene, *Hoxa3*, results in anomalies of carotid arteries, deriving from the 3rd PAAs (Chisaka and Capecchi, 1991; Kameda et al., 2003). The lack of more severe cardiac malformations in *Hoxa1* and *Hoxa3* mutant mice indicates that functional redundancy may be at play. Interestingly, Soshnikova N et al. recently showed that deletion of either the *HoxA* or *HoxB* cluster did not result in a heart defect (Soshnikova et al., 2013). It

* Corresponding author to: Aix Marseille Université, INSERM, GMGF UMR_S910, Faculté de Médecine, 27 Bd Jean Moulin, 13005 Marseille, France.
E-mail address: stephane.zaffran@univ-amu.fr (S. Zaffran).
[1] Present address: M.R.: Laboratory of Genetics and Development, Institut de Recherches Cliniques de Montréal (IRCM), Université de Montréal, Montréal Québec, Canada.
[2] Present address: B.L.: The University of Chicago, Department of Pediatrics, 900 East 57th street, Chicago, Illinois 60637.
[3] Present address: N.B.: Aix Marseille Univ, CNRS, IBDM, Marseille, France.

was only when both the *HoxA* and *HoxB* clusters were deleted together that they observed an aggravated phenotype, where the heart failed to undergo looping. Furthermore, our recent works showed that paralogous *Hoxa1* and *Hoxb1* genes are expressed in cardiac progenitors contributing to arterial pole of the heart where they play a redundant role for correct OFT development (Bertrand et al., 2011; Roux et al., 2015).

Previous studies have demonstrated extensive overlapping function between *Hoxa1* and *Hoxb1* during pre-otic hindbrain specification (Gavalas et al., 1998; Rossel and Capecchi, 1999; Studer et al., 1998). We hypothesized that absence of both *Hoxa1* and *Hoxb1* genes may also have consequences on the development of PAAs, and subsequent great arteries. In the present study, we examined the possible synergy between *Hoxa1* and *Hoxb1* during PAA development through the analysis of allelic combinations. A genetic lineage tracing analysis with *Hoxa1-enhIII-Cre* and *Hoxb1*$^{IRES\text{-}Cre}$ mice showed that both genes are expressed in cardiac NCC progenitors invading the pharyngeal region. In addition, our work revealed, for the first time, that great artery defects are observed at low penetrance in embryos with loss of *Hoxb1* function. The phenotypic manifestations became more severe in the context of the additional inactivation of one *Hoxa1* allele, demonstrating that *Hoxa1* and *Hoxb1* synergize in a dosage-dependent manner during PAA development. Our analysis suggests that abnormal cardiac NCC migration is at the origin of these anomalies. We conclude that *Hoxa1* and *Hoxb1* have overlap of functions in the patterning of the rhombomeres where cardiac NCCs arise. *Hoxa1* and *Hoxb1* mutant mice thus provide a model for PAA defects often observed in CHDs.

2. Results

2.1. Hoxa1 and Hoxb1 affect great artery formation

Although *Hoxb1* is expressed in the rhombomere (r) 4 and in neural crest structures derived from the 2nd branchial arch, previous studies have not described pharyngeal arch artery (PAA) defects in *Hoxb1*-null mice (Gaufo et al., 2000; Goddard et al., 1996; Studer et al., 1996). Our recent analysis of cardiac malformations in *Hoxb1*$^{-/-}$ embryos revealed that some mutant embryos had anomalies of the OFT including misalignment and ventricular septal defects (VSD) (Roux et al., 2015). To determine if the lack of *Hoxb1* affects also great artery development

Table 1
Hoxa1 and *Hoxb1* synergistically regulate cardiovascular development.

Genotype	*n*	Abnormal (n)	IAA-B	CAA	Ab-RSA	RAA
Wild-type	38	0	–	–	–	–
Hoxb1$^{+/-}$	28	0	–	–	–	–
Hoxb1$^{-/-}$	28	4% (1)	4% (1)	–	–	–
Hoxa1$^{+/-}$	34	0	–	–	–	–
Hoxa1$^{-/-}$	27	81% (22)	37% (10)	26% (7)	15% (4)	18% (5)
Hoxa1$^{+/-}$;*Hoxb1*$^{+/-}$	24	21% (5)	12% (3)	–	8% (2)	–
Hoxa1$^{+/-}$;*Hoxb1*$^{-/-}$	12	42% (5)	17% (2)	17% (2)	8% (1)	8% (1)
Hoxa1$^{-/-}$;*Hoxb1*$^{+/-}$	11	82% (9)	64% (7)	9% (1)	18% (2)	9% (1)
Hoxa1$^{-/-}$;*Hoxb1*$^{-/-}$	3	100% (3)	100% (3)	–	67% (2)	–

"Abnormal" corresponds to the total number of embryos with great artery defects. Ab-RSA, aberrant origin of the right subclavian artery including retroesophageal right subclavian artery; CAA, cervical aortic arch; IAA-B, interrupted aortic arch type B; RAA, right side aortic arch; VSD, ventricular septal defect.

we further examined *Hoxb1*$^{-/-}$ embryos at fetal stages. All wild-type (*WT*) embryos (n = 38) had normal great arteries, whereas we found a low penetrance (4%; 1 out of 28) of interruption of the aortic arch type B (IAA-B) in *Hoxb1*$^{-/-}$ embryos (Fig. 1A and B; Table 1). Since *Hoxa1* and *Hoxb1* have overlapping roles during hindbrain development, we tested for functional redundancy of the two genes in great artery development by intercrossing *Hoxa1*$^{+/-}$;*Hoxb1*$^{+/-}$ heterozygous mice (Table S1). At E17.5, all genotypes were recovered according to Mendelian ratios with the exception of *Hoxa1*$^{-/-}$;*Hoxb1*$^{-/-}$ genotype, suggesting an early lethality of double mutant embryos ($p < 0.05$ using Fisher's test, Table S1). This observation is consistent with previous studies showing a lethality of *Hoxa1*$^{-/-}$;*Hoxb1*$^{-/-}$ mouse embryos (Gavalas et al., 1998; Rossel and Capecchi, 1999). In line with a recent study, 81% of *Hoxa1*$^{-/-}$ embryos exhibited anomalies of the great arteries (Table 1) (Makki and Capecchi, 2012). These defects include IAA-B (10/27; Fig. 1C), cervical aortic arch (CAA; 7/27; Fig. 1D), aberrant retro-esophageal right subclavian artery (Ab-RSA; 4/27) and right side aortic arch (RAA; 5/27). Gross morphological observations did not reveal any difference in the great arteries of single heterozygous *Hoxa1*$^{+/-}$ or *Hoxb1*$^{+/-}$ compared to *WT* littermates. However, we found that five out of twenty-four *Hoxa1*$^{+/-}$;*Hoxb1*$^{+/-}$ embryos (21%) had great artery defects (Fig. 1E; Table 1). Interestingly, when one functional allele of *Hoxa1* was removed from a *Hoxb1*$^{-/-}$ background the number of great artery anomaly was greatly increased

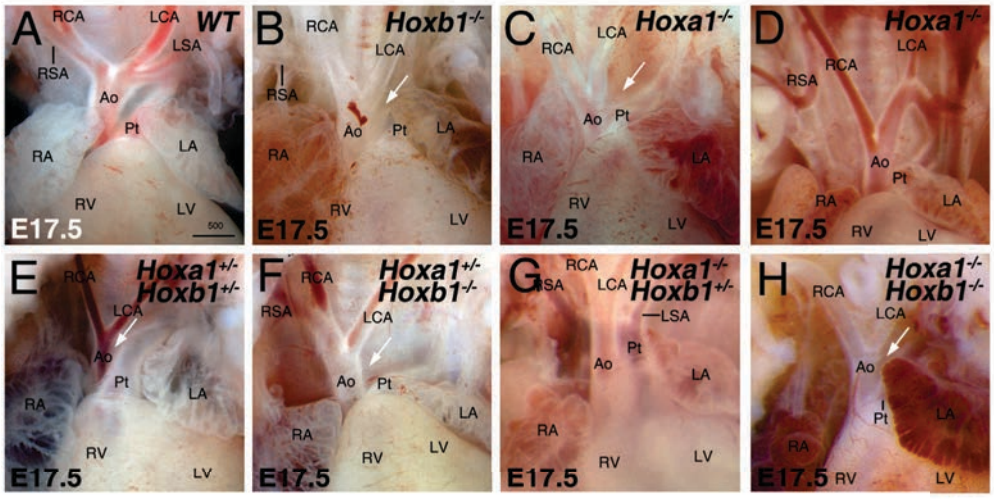

Fig. 1. Cardiovascular abnormalities in *Hoxb1*$^{-/-}$, *Hoxa1*$^{-/-}$ and compound *Hoxa1*; *Hoxb1* mutants. (A–H) Frontal views of wild-type (*WT*; A), *Hoxb1*$^{-/-}$ (B), *Hoxa1*$^{-/-}$ (C,D), *Hoxa1*$^{+/-}$;*Hoxb1*$^{+/-}$ (E), *Hoxa1*$^{+/-}$;*Hoxb1*$^{-/-}$ (F), *Hoxa1*$^{-/-}$;*Hoxb1*$^{+/-}$ (G), and *Hoxa1*$^{-/-}$;*Hoxb1*$^{-/-}$ (H) hearts at E17.5. (A) Normal pattern of the aortic arch in wild-type embryo. (B) *Hoxb1*$^{-/-}$ embryo with interrupted aortic arch type-B (IAA-B). (C, D) *Hoxa1*$^{-/-}$ embryos displaying aortic arch defects including IAA-B (C) and cervical aortic arch (D) associated with aberrant right subclavian artery (Ab-RSA). (E–H) compound *Hoxa1*;*Hoxb1* mutants showing IAA-B defects. Note the right aortic arch (RAA) in *Hoxa1*$^{-/-}$;*Hoxb1*$^{+/-}$ (G) embryo. Arrows points IAA-B defects. Ao: aorta; LCA: left carotid artery; LSA: left subclavian artery; LV: left ventricle; Pt: pulmonary trunk; RCA: right carotid artery; RSA: right subclavian artery; RV: right ventricle. Scale bar: 500 μm.

(Fig. 1G; Table 1). Indeed, 42% of abnormal *Hoxa1*$^{+/-}$;*Hoxb1*$^{-/-}$ embryos were observed instead of 4% in a *Hoxb1*$^{-/-}$ background. Our observations revealed that the great artery phenotype of *Hoxa1*$^{-/-}$ was greatly exacerbated when one functional allele of *Hoxb1* was removed. This combination generated more IAA-B and less CAA than homozygous *Hoxa1* mutant alone (Table 1). In addition, we observed more IAA-B associated with Ab-RSA in *Hoxa1*$^{-/-}$;*Hoxb1*$^{+/-}$ than *Hoxa1*$^{-/-}$ embryos (Table 1). Furthermore, all double homozygous embryos showed IAA-B associated in 67% of case with Ab-RSA (Fig. 1H; Table 1). These data suggest that *Hoxa1* and *Hoxb1* have overlapping functions during early development of the great arteries.

2.2. Hoxa1 and Hoxb1 interact in vivo during the development of the 4th PAA

As described above, *Hoxa1* and *Hoxb1* mutant fetuses displayed great artery defects including Ab-RSA, either alone or combined with IAA-B, suggestive of a failure of the 4th PAAs (Hutson and Kirby, 2007). In order to analyze PAA development we injected India ink into the heart of compound mutant embryos at E10.5 (Figs. 2 and 3). *WT* (n = 8), *Hoxa1*$^{+/-}$ (n = 12), *Hoxb1*$^{+/-}$ (n = 12) and *Hoxb1*$^{-/-}$ (n = 7) embryos had normal PAA development (Figs. 2A, B, F and 3A, B, C, F). All *Hoxa1*$^{-/-}$ embryos (n = 6) had abnormal 4th PAA on one or both side of the embryo (Figs. 2E and 3G). Interestingly, the removal of at least one allele of *Hoxb1* in the *Hoxa1*$^{+/-}$ heterozygote background caused abnormal 4th PAA development (Figs. 2C, D and 3D, E). The low penetrance of the 4th PAA phenotype found in *Hoxa1*$^{+/-}$;*Hoxb1*$^{+/-}$ embryos at E10.5 (33%; Table S2) was slightly higher than the percentage of defects found at E17.5 from same genotype (21%, Table S2). This difference is likely to be due to recovery from arterial growth delay as previously observed for other mutant mice (Lindsay and Baldini, 2001). Furthermore, dosage reduction of at least one copy of *Hoxb1* in a *Hoxa1*$^{-/-}$ background increased the penetrance and the severity of the 4th PAA phenotype (Figs. 2E, G, H, and 3G, H, I). All double mutant embryos had bilateral defects of the 4th PAAs associated with an absence of the 6th PAAs, suggesting that the 4th and 6th pharyngeal arches were dramatically affected in *Hoxa1*$^{-/-}$;*Hoxb1*$^{-/-}$ embryos (Figs. 2H and 3I). Overall, our results demonstrate that *Hoxa1* and *Hoxb1* interact genetically during PAA development.

2.3. Structures derived from the 4th PAAs are deficient in compound Hoxa1;Hoxb1 embryos

We next investigated PAA formation defects found in single and compound mutants at the cellular level. We evaluated vascular smooth muscle differentiation by immunohistochemistry using an antibody directed against smooth muscle α-actin (αSMA) in *WT* and single or compound *Hox* mutant embryos. At E10.5, the 3rd PAA served as an internal control for αSMA-labeling. Consistent with results obtained from India ink injections, we found that at E10.5 the 4th PAA walls of *WT*, *Hoxb1*$^{+/-}$ and *Hoxb1*$^{-/-}$ embryos were SMA positive (Fig. 4A, B, F), whereas *Hoxa1*$^{-/-}$, and compound *Hoxa1*;*Hoxb1* mutant embryos had no αSMA-labeled cells in the walls of the hypoplastic 4th PAA (Fig. 4C, D, E, G, H). We conclude that the 4th PAA phenotype observed in these mutant embryos at E10.5 is associated with abnormal differentiation of vascular smooth muscles of the vascular walls. However, the differentiation defect cannot be attributed to absence of endothelial cells since immunohistochemistry with the endothelial marker Pecam demonstrated that these cells were detected in the 4th PAA, although a small vessel lumen was observed (Fig. 4I–P).

In conclusion, although loss of *Hoxb1* function alone had no apparent effect on 4th PAA development, reduction of *Hoxa1* gene dosage uncovered a contribution of *Hoxb1* to this PAA and its derived-structures.

2.4. Hoxa1 and Hoxb1 are required for cardiac neural crest cell migration

In order to investigate the origin of the 4th PAA abnormalities, we evaluated the contribution of *Hoxa1*- and *Hoxb1*-derived cells to the 3rd and 4th–6th PAA. Thus, we performed a lineage-tracing analysis using *Hoxa1-enhIII-Cre* and *Hoxb1*$^{IRES\text{-}Cre}$ transgenic and knock-in mice respectively (Arenkiel et al., 2003; Li and Lufkin, 2000). As previously reported, X-gal staining in *Hoxa1-enhIII-Cre*;*R26R* embryos was less intense and robust than in *Hoxb1*$^{IRES\text{-}Cre}$;*R26R* embryos (Bertrand et al., 2011). Despite slight differences, both *Hoxa1-Cre* and *Hoxb1-Cre* labeled cells were detected in the 3rd and 4th–6th pharyngeal arches of E10.5 *Hoxa1-enhIII-Cre*;*R26R* and *Hoxb1*$^{IRES\text{-}Cre}$;*R26R* embryos respectively (Fig. 5A–D, asterisks). Sections revealed X-gal-positive cells in pharyngeal ectoderm and endoderm, as well as mesenchyme NCCs (Fig. 5C, D). At E12.5, *Hoxa1-Cre* and *Hoxb1-Cre* labeled cells invaded the endocardial cushions of the OFT, suggesting that *Hoxa1*- and *Hoxb1*-lineages

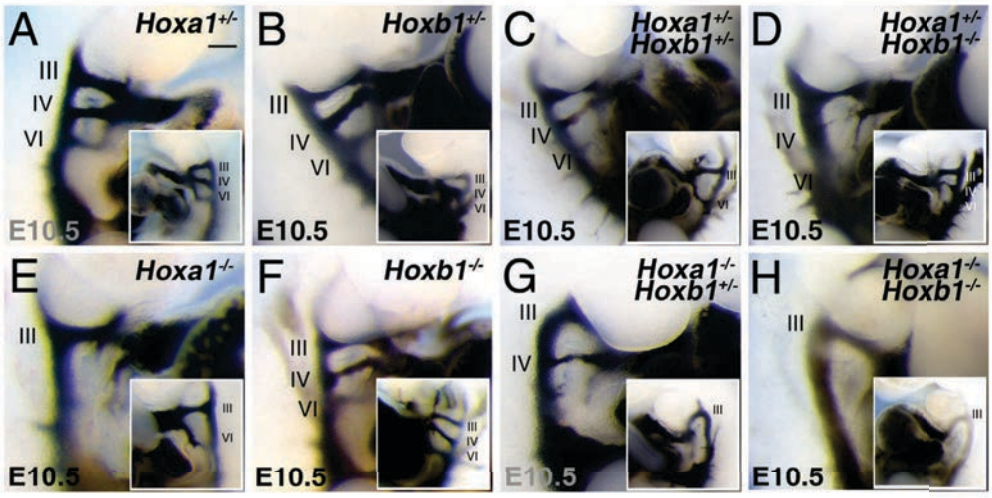

Fig. 2. Pharyngeal arch artery defects in compound *Hoxa1*;*Hoxb1* mutant embryos. (A–H) Right and left lateral views of embryos injected with India ink at E10.5. Normal formation of the 3rd, 4th and 6th pharyngeal arch artery (PAA) is observed in *Hoxa1*$^{+/-}$ (A), *Hoxb1*$^{+/-}$ (B) and *Hoxb1*$^{-/-}$ (F) embryos, whereas defects of the 4th and/or 6th PAA are observed in *Hoxa1*$^{-/-}$ (E), and compound *Hoxa1*;*Hoxb1* mutants (C, D, G, H). Defects include absence of the left 4th PAA in a *Hoxa1*$^{+/-}$;*Hoxb1*$^{+/-}$ double heterozygote embryo (C), bilateral hypoplastic 4th and 6th PAA in a *Hoxa1*$^{+/-}$;*Hoxb1*$^{-/-}$ embryo (D), bilateral absence of the 4th PAA in *Hoxa1*$^{-/-}$ embryos (E), bilateral hypoplastic 4th right PAA and absence of the 4th left PAA in *Hoxa1*$^{-/-}$;*Hoxb1*$^{+/-}$ embryos (G) and bilateral absence of the 4th and 6th PAA in *Hoxa1*$^{-/-}$;*Hoxb1*$^{-/-}$ embryos (H). III, 3rd pharyngeal arch artery; IV, 4th pharyngeal arch artery; VI, 6th pharyngeal arch artery. Scale bar: 100 μm.

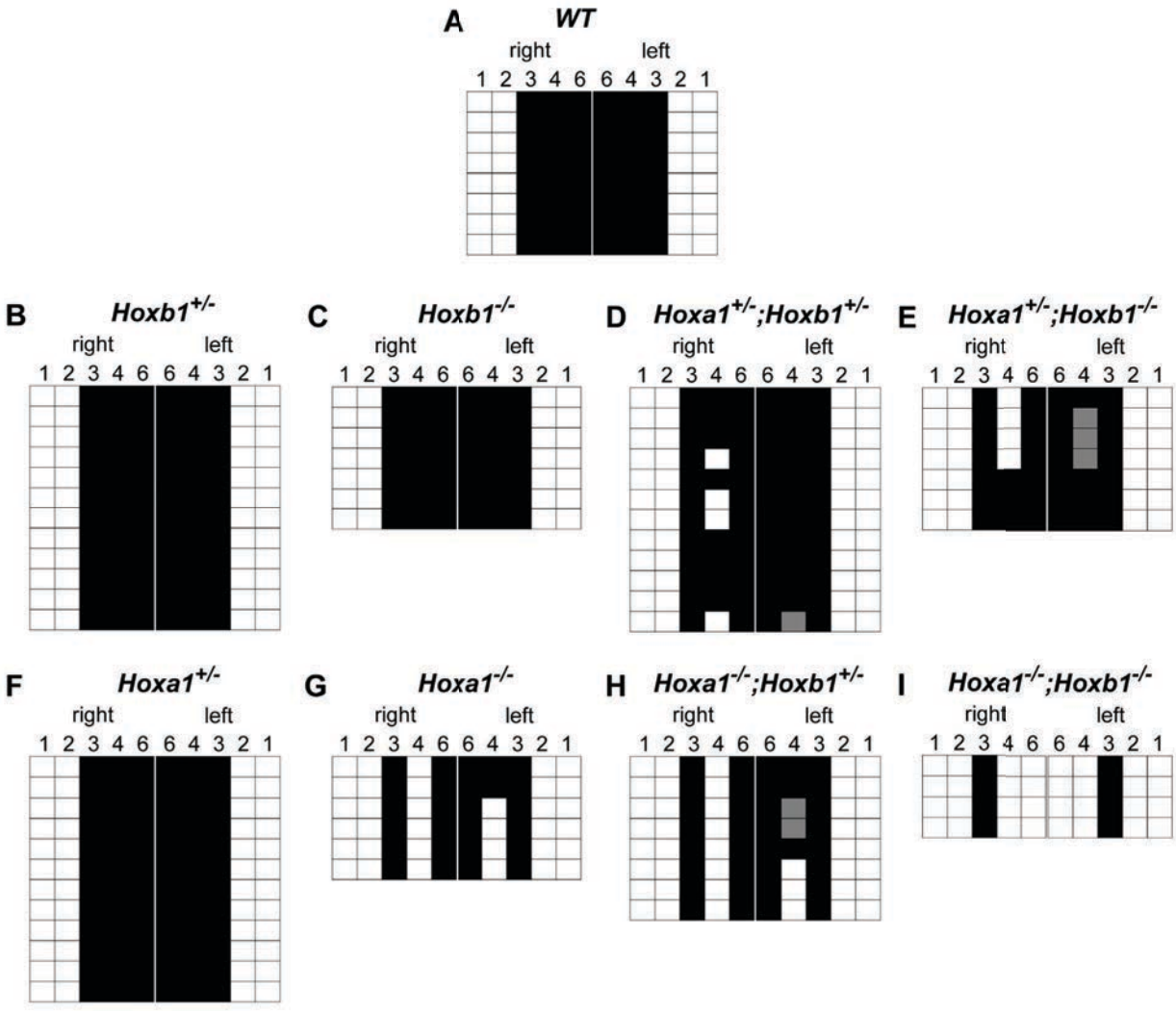

Fig. 3. Summary of pharyngeal arch artery defects. (A–I) Summary of ink injection for wild-type (*WT*; A), *Hoxb1*$^{+/-}$ (B) *Hoxb1*$^{-/-}$ (C), *Hoxa1*$^{+/-}$;*Hoxb1*$^{+/-}$ (D), *Hoxa1*$^{+/-}$;*Hoxb1*$^{-/-}$ (E), *Hoxa1*$^{\pm}$ (F), *Hoxa1*$^{-/-}$ (G), *Hoxa1*$^{-/-}$;*Hoxb1*$^{+/-}$ (H) and *Hoxa1*$^{-/-}$;*Hoxb1*$^{-/-}$ (I) embryos at E10.5. Each line represents the analysis of one embryo. Black boxes indicate pharyngeal arch arteries (PAA) labeled by ink, and white boxes, PAA not labeled by ink. Grey boxes indicate weakly labeled PAA.

contribute to cardiac NCCs (Fig. 5E, F). These results are consistent with a previous work describing expression of *Hoxa1* and *Hoxb1* in the forming hindbrain of E7.75 embryos (Murphy and Hill, 1991), where cardiac NCCs arise (Kirby, 2007), suggesting that both *Hoxa1* and *Hoxb1* genes are expressed in precursors of cardiac NCCs that contribute to the 3rd and 4th–6th pharyngeal arches and OFT development.

To examine the migration of cardiac NCCs in *Hoxa1* and *Hoxb1* deficient embryos, we performed whole mount *in situ* hybridization at E9.5 for *Crabp1* and *Sox10*, markers of migrating NCCs (Kuhlbrodt et al., 1998; Maden et al., 1992). Two streams of cells were observed in *WT*, *Hoxa1*$^{+/-}$, *Hoxb1*$^{+/-}$ and *Hoxb1*$^{-/-}$ embryos (Figs. 5 and 6A, B, D, G, H, J). In contrast, these streams were partially or completely fused in *Hoxa1*$^{-/-}$ embryos (Fig. S1; compare yellow (normal) and red (abnormal) arrowheads). Despite the absence of NCC phenotypes in *Hoxb1*$^{+/-}$ and *Hoxb1*$^{-/-}$ embryos (Fig. 6B, D, H, J), cardiac NCC migration defects were observed as *Hoxa1* gene dosage was reduced in the same genetic background (Fig. 6C, E, I, K), consistent with the great artery phenotypes observed at a later stage (Table 1). Furthermore, the NCC migration defect was more severe when both *Hoxa1* and *Hoxb1* were absent (Fig. 6F, L). We conclude that the removal of at least one functional allele of *Hoxa1* from a *Hoxb1*$^{-/-}$ background is sufficient to affect the migration of NCCs in the pharyngeal arches, suggesting that loss of *Hoxb1* function is rescued by the presence of *Hoxa1*, as previously described for other tissues.

Previous studies have demonstrated that *Hoxa1* and *Hoxb1* play critical role in the specification of rhombomeres where NCCs arise (Makki and Capecchi, 2012; Rossel and Capecchi, 1999). In order to determine whether specification of the neural crest is affected in compound *Hoxa1*;*Hoxb1* mutant embryos, we performed *in situ* hybridization for *Zic1* transcripts a marker of the neural plate border (Aruga, 2004). We found that *Zic1* expression was strongly down-regulated in the posterior hindbrain of *Hoxa1*$^{+/-}$;*Hoxb1*$^{-/-}$, *Hoxa1*$^{-/-}$;*Hoxb1*$^{+/-}$ and *Hoxa1*$^{-/-}$;*Hoxb1*$^{-/-}$ compared to single mutant embryos at E8.5 (Fig. 7). Interestingly, we found that expression of *Krox20*, marking r3 and r5, was largely reduced in r5 in *Hoxa1*$^{+/-}$;*Hoxb1*$^{+/-}$ embryos, suggesting an anomaly in the regional identity of the neural crest population (Fig. S2). Altogether these data confirm an overlap of functions between *Hoxa1* and *Hoxb1* during neural crest specification.

3. Discussion

3.1. Overlapping functions of Hoxa1 and Hoxb1 during pharyngeal arch artery and great artery patterning

Our current study extends the role of *Hoxa1* and *Hoxb1* to events occurring during patterning of the pharyngeal arch arteries (PAAs) and subsequent formation of the great arteries. The development of the 3rd, 4th and 6th PAAs is crucial for great artery patterning. Defective

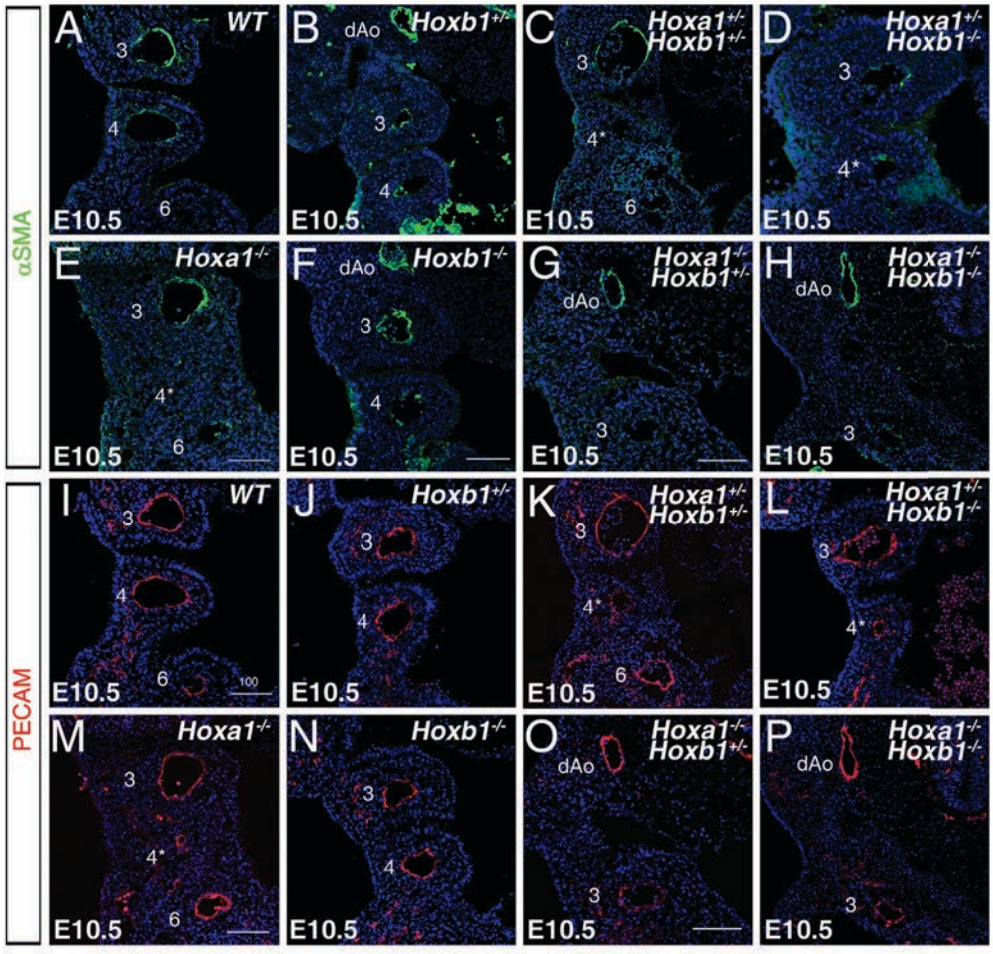

Fig. 4. Vascular smooth muscle differentiation and endothelial cells in single and compound *Hoxa1*;*Hoxb1* mutant embryos. (A–H) Immunohistochemistry with *anti*-αSMA (green) and PECAM (red) on frontal sections through the pharyngeal region showing vascular smooth muscles of the vessels in single and compound mutant embryos at E10.5. Vessels of the 4th PAA in *Hoxa1*$^{+/-}$;*Hoxb1*$^{+/-}$ (C), *Hoxa1*$^{+/-}$;*Hoxb1*$^{-/-}$ (D), *Hoxa1*$^{-/-}$ (E), *Hoxa1*$^{-/-}$;*Hoxb1*$^{+/-}$ (G), and *Hoxa1*$^{-/-}$;*Hoxb1*$^{-/-}$ (H) are devoid of vascular smooth muscles. The vessel wall of the 3rd PAA served as a control. Endothelial cells detected with anti-PECAM are not affected in hypoplastic 4th PAA (asterisk) in *Hoxa1*$^{+/-}$;*Hoxb1*$^{+/-}$ (K), *Hoxa1*$^{+/-}$;*Hoxb1*$^{-/-}$ (L), and *Hoxa1*$^{-/-}$ (M). Note the presence of a single PAA in *Hoxa1*$^{-/-}$;*Hoxb1*$^{\pm}$ (O) and *Hoxa1*$^{-/-}$;*Hoxb1*$^{-/-}$ (P) embryos. Scale bars: 100 μm.

development of the 4th PAAs underlies severe vascular anomalies, such as interrupted aortic arch type B (IAA-B), which is lethal at birth (Plein et al., 2015). IAA-B defect was identified in a large number of *Hoxa1*$^{-/-}$ and compound *Hoxa1*;*Hoxb1* mutant embryos (Table 1; (Makki and Capecchi, 2012)), which was confirmed by 4th PAA anomalies found in corresponding mutant embryos at E10.5 (Table S2). Loss of *Hoxa1* or *Hoxb1* function has different consequence on 4th PAA formation. Indeed, all *Hoxa1*$^{-/-}$ embryos showed 4th PAA anomaly, while disruption of *Hoxb1* did not, or only slightly, alter the patterning of PAAs, suggesting a major role of *Hoxa1* and minor role for *Hoxb1* in the formation of the PAAs. However, our cross-breeding experiments showed a synergistic interaction of *Hoxa1* and *Hoxb1* during PAA development, causing 4th PAA defects in compound *Hoxa1*;*Hoxb1* heterozygous embryos, and significant enhancement of the phenotype by the disruption of one, or two allele(s) of *Hoxb1* in the *Hoxa1*-null background. Strikingly, double *Hoxa1*$^{-/-}$;*Hoxb1*$^{-/-}$ embryos had bilateral defects of the 4th and 6th PAAs, suggesting that the morphology of caudal pharyngeal arches could be abnormal in complete absence of *Hoxa1* and *Hoxb1*. Rossel and Capecchi, (1999) have shown that the 2nd pharyngeal arch is completely missing in *Hoxa1*$^{-/-}$;*Hoxb1*$^{+/-}$ and *Hoxa1*$^{-/-}$;*Hoxb1*$^{-/-}$ embryos, and that this defect is associated with the loss of r4 and r5 domains (Rossel and Capecchi, 1999). Furthermore, the morphology of the 3rd pharyngeal pouch is also perturbed in the double mutant embryos, suggesting a broader disturbance of the arch tissues. Thus, we cannot exclude that absence of vessels in the 4th and 6th arches was caused by a deficiency in others arch tissues.

Our study confirms previous work demonstrating overlap of function between these paralogous *Hox* genes (Gavalas et al., 1998; Rossel and Capecchi, 1999; Roux et al., 2015; Soshnikova et al., 2013).

3.2. Hoxa1 and Hoxb1 are required for cardiac NCC specification

Developmental failure of the 4th PAAs causes great artery defects such as IAA-B and Ab-RSA. Several studies have shown that NCCs contribute to the formation of the 4th PAAs (see (Kirby, 2007)). Our genetic lineage tracing revealed that *Hoxa1* and *Hoxb1* genes are expressed in cardiac NCCs that invade the pharyngeal region and subsequently the OFT. Consistently, analysis of NCC markers indicated an abnormal migration of cardiac NCCs in single *Hoxa1* mutant as well as in compound *Hoxa1*;*Hoxb1* mutant embryos, suggesting a mis-specification of neural crest in these embryos. In fact, a previous study has reported that *Hoxa1* and *Hoxb1* are necessary for specification of rhombomeres 3 to 5 (Rossel and Capecchi, 1999). Interestingly, single *Hoxa1*-null mutant embryos showed metameric disorganization of the developing hindbrain, while *Hoxb1* mutation affected only the fate of neurons within r4 (Carpenter et al., 1993; Goddard et al., 1996; Lufkin et al., 1991; Studer et al., 1996). Rossel and Capecchi have proposed that the phenotypic differences between *Hoxa1*$^{-/-}$ and *Hoxb1*$^{-/-}$ embryos are not caused by

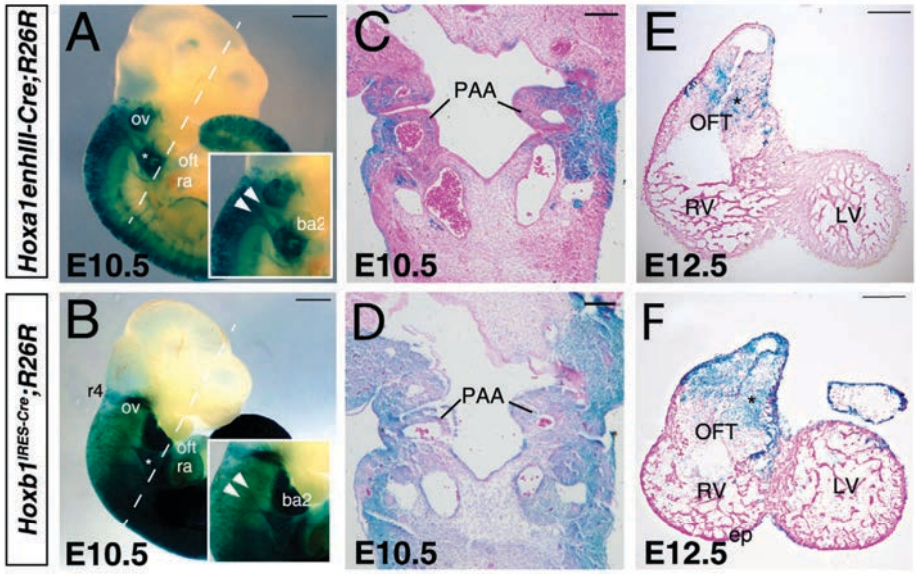

Fig. 5. Genetic lineage analysis reveals contribution of *Hoxa1*$^{+}$ and *Hoxb1*$^{+}$ cells to the endocardial cushions of the outflow tract. (A–F) *Hoxa1*- and *Hoxb1*-lineage are visualized by X-gal staining on *Hoxa1-enhIII-Cre*; *R26R* and *Hoxb1*$^{IRES\text{-}Cre}$;*R26R* embryos. (A, B) Lateral view of X-gal stained embryos at E10.5. *Hoxa1*- and *Hoxb1*-positive cells are observed in the 3rd, 4th and 6th pharyngeal arches (asterisks). Insets show a higher magnification of the pharyngeal region (arrowheads indicate migration of neural crest cells to the PAAs). (E, F) Transverse sections of X-gal stained heart at E12.5, showing labeled cells in the endocardial cushions of the outflow tract (asterisks). ba2, branchial arch 2; ep, epicardium; LV, left ventricle; OFT, outflow tract; ov, otic vesicle; PAA, pharyngeal aortic arch; r4, rhombomere 4; RV, right ventricle. Scale bars: 500 μm (A, B); 100 μm (C, D); 200 μm (E, F).

separate protein functions, but rather from differences in the initial expression of these genes (Rossel and Capecchi, 1999). Indeed, *Hoxa1* is expressed first in the prospective r3-r4 boundary, where it participates in the activation of *Hoxb1* (Forlani et al., 2003; Goddard et al., 1996; Murphy and Hill, 1991; Studer et al., 1998; Studer et al., 1996). Interestingly, we identified a down-regulation of *Krox20* expression in r5 in compound *Hoxa1*;*Hoxb1* heterozygous embryos, suggesting that reduction of Hoxa1/Hoxb1 function is sufficient to disrupt the specification of the r5. Our analysis of *Crabp1* and *Sox10* expression revealed abnormal post-otic streams of migrating cardiac NCCs in compound *Hoxa1*;*Hoxb1* embryos, suggesting that more caudal rhombomeres are also altered in this genetic context.

Cardiac NCCs are important for great artery patterning but also for proper septation of the OFT (Kirby et al., 1983). Our recent work has demonstrated that both *Hoxa1* and *Hoxb1* function are required in the second heart field during heart development (Bertrand et al., 2011; Roux et al., 2015). Indeed, a low frequency of VSD was observed in *Hoxa1*- and *Hoxb1*-null mutants, 11% and 21% respectively. However, our recent work has demonstrated that OFT septation was not altered in *Hoxa1*$^{-/-}$ mutant embryos, suggesting uncoupling between PAA patterning and OFT defects. This is supported by experiments in the chick, which has demonstrated that abnormal great artery patterning does not necessarily lead to OFT malformations (Kirby et al., 1997). Interestingly, immunostaining with AP-2α did not reveal obvious difference in the number of NCCs that invading the OFT of *Hoxa1*$^{-/-}$ embryos, suggesting that cardiac NCC populate the pharyngeal region in proximity of the OFT (Roux et al., 2015). The first NCCs to invade the OFT participate in the formation of the aortico-pulmonary septum, whereas those migrating later contribute to PAA remodeling, in particular to the smooth muscle wall of the arteries themselves (Boot et al., 2003). However, heterochronic transplantation experiments in this study showed that the late migrating NCCs were not developmentally restricted and in absence of the "early-migrating" cells, they could invade the aortico-pulmonary septum. Thus, surrounding NCCs might compensate for the defect of a specific group of NCCs. We hypothesize that loss of *Hoxa1* affects particularly the specification of premigratory cardiac NCCs as its anterior limit of expression reaches the hindbrain at E8, before regressing caudally by E8.5 (Murphy and Hill, 1991), and that part of *Hoxa1*-expressing NCCs migrate to caudal pharyngeal arches. *Hoxb1*$^{-/-}$ embryos have never been described to have abnormalities in cardiac neural crest-derived tissues (Gaufo et al., 2000; Goddard et al., 1996; Studer et al., 1996). However, we have observed one *Hoxb1* mutant embryo with aortic arch artery defect such as IAA-B (Table 1), which is characteristic of a developmental failure of the left 4th PAA. Such anomaly could be caused by defects in the pharyngeal surface ectoderm, mesoderm, or endoderm, as well as abnormal NCC migration. The C57Bl/6 background of the *Hoxb1*^{GFP} allele used in our study has probably contributed to reveal such phenotype. However, we cannot exclude that the single abnormal embryo observed out of twenty-eight embryos was due to this specific background. *Hoxb1*$^{-/-}$ embryos did not have abnormal 4th PAAs after ink injection at E10.5 or a cardiac NCC migratory defect, confirming a very low penetrance of this anomaly. A significant fraction of compound *Hoxa1*;*Hoxb1* mutants, on the contrary, show an aortic arch artery phenotype. Interestingly, the severity of aortic arch artery defect is linked to the number of alleles deleted in compound mutant embryos. The percentage of embryos with IAA-B *versus* CAA is directly correlated with the genotype of compound mutant embryos. Aortic arch artery remodeling has been shown to result from a reduced number of NCCs reaching the 4th PAAs (Calmont et al., 2009). We provide evidence that migrating streams of cardiac NCCs are disorganized in single *Hoxa1*$^{-/-}$ embryos, and that this phenotype is aggravated in the compound mutant embryos. Thus, the absence of *Hoxa1* and *Hoxb1* in the hindbrain domain leads to a dysregulation of migratory path-finding of cardiac NCCs and probably a reduction of the number of these cells reaching the caudal PAAs, leading to aortic arch artery defects. The migration defect could also be caused by misexpression of factors required during migration of NCCs. Interestingly, Zic1, which is down-regulated in *Hoxa1*-null embryos (Makki and Capecchi, 2012), but also in compound *Hoxa1*;*Hoxb1* mutant embryos (Fig. 7), was shown to interact with Gbx2, a factor required in the pharyngeal surface ectoderm for the migration of the cardiac NCCs (Calmont et al., 2009; Li et al., 2009).

In summary, our data suggest that both *Hoxa1* and *Hoxb1* genes are important for PAA formation through their influence on cardiac NCCs, providing a model to study the molecular origin of great artery defects often observed in human patients.

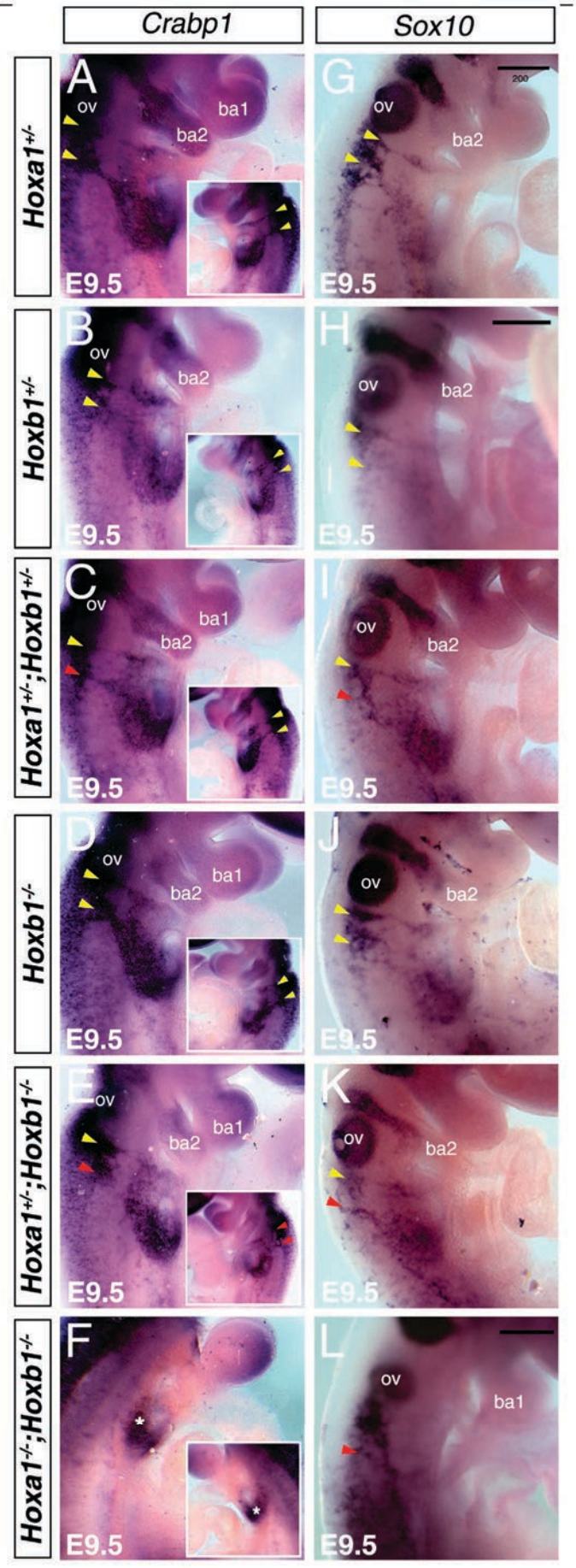

4. Material and Methods

4.1. Mice

All mouse experiments were done under protocols approved by the "comité d'éthique pour l'expérimentation animale" (Marseille ethical committee, Protocol N°32-08102012). The null alleles of *Hoxa1*^{neo} and *Hoxb1*^{GFP} (hereafter referred to as *Hoxa1*$^{-}$ and *Hoxb1*$^{-}$) have been already described (Gaufo et al., 2000; Lufkin et al., 1991). To avoid strain background effects, we used mice crossed onto the C57BL/6 background. Double heterozygous *Hoxa1*$^{+/-}$;*Hoxb1*$^{+/-}$ mice were interbred to obtain *Hoxa1*$^{-/-}$;*Hoxb1*$^{-/-}$ embryos (Table S1). *Hoxb1*$^{IRES\text{-}Cre}$ knock-in mouse line, and *Hoxa1-enhIII-Cre* and *Rosa26*^{LacZ} (*R26R*) transgenic lines have been previously described (Arenkiel et al., 2003; Li and Lufkin, 2000; Soriano, 1999). Mice were genotyped by PCR and embryos staged taking the morning of the vaginal plug as embryonic day E0.5.

4.2. RNA in situ hybridization and X-gal staining

To visualize β-galactosidase activity, embryos or hearts were isolated, fixed in 4% paraformaldehyde for 20 min and placed in X-gal solution, according to standard procedures. Embryos or hearts were photographed (Zeiss Axiozoom) as whole-mount specimens and then embedded in paraffin and cut at 8 μm per tissue sections before being counterstained with eosin.

Whole-mount *in situ* hybridization (ISH) was performed as previously described (Ryckebusch et al., 2010). The following riboprobes used in this study were *Crabp1*, *Krox20*, *Sox10*, and *Zic1*. For ISH, hybridization signals were then detected by alkaline phosphatase (AP)-conjugated anti-DIG antibodies (1/2000; Roche), which were followed by color development with NBT/BCIP (magenta) substrate (Promega). After staining, the samples were washed in PBS and post-fixed. Embryos were photographed using a Zeiss Axiozoom coupled to an Axiocam digital camera (AxioVision 4.4, Zeiss). The number of embryos examined was at least 3 for each genotype.

4.3. Ink injections

For India ink injection, embryos were collected at E10.5 and injected intracardially using drawn Pasteur pipettes. Seventy-six embryos resulting from intercrosses between double heterozygous *Hoxa1*$^{+/-}$;*Hoxb1*$^{+/-}$ mice were scored. Injected embryos were subsequently fixed in PBS-buffered 4% paraformaldehyde. PAA anatomy was analyzed by visual inspection after clearing with PBS. In some cases, embryos were processed for immunohistochemistry after ink injection.

4.4. Immunohistochemistry

Standard immunohistochemistry procedures were used as previously described (Roux et al., 2015). Whole-mount specimens were embedded in OCT and cut at 12 μm per tissue section. α-SMA (1:500, Sigma), CD31 (PECAM) (1:100, Pharmingen), immunohistochemistry were performed using 4% paraformaldehyde fixed tissue and Alexa fluorescent-conjugated antibodies (Life Technologies) were used at 1:500. The number of embryos examined was at least 3 for each genotype.

Fig. 6. Cardiac neural crest cells migration defects in compound *Hoxa1*; *Hoxb1* mutant embryos. (A–L) Whole-mount *in situ* hybridization for *Crabp1* (A–F) and *Sox10* (G–L) transcripts (marking neural crest cells) in *Hoxa1*$^{+/-}$ (A, G), *Hoxb1*$^{+/-}$ (B, H), *Hoxa1*$^{+/-}$;*Hoxb1*$^{+/-}$ (C, I), *Hoxb1*$^{-/-}$ (D, J), *Hoxa1*$^{\pm}$;*Hoxb1*$^{-/-}$ (E, K) and *Hoxa1*$^{-/-}$;*Hoxb1*$^{-/-}$ (F, L) mutants at E9.5. Normal migration of NCCs to the 3rd and 4th PAA (yellow arrowheads) is observed in *Hoxa1*$^{+/-}$ (A, G), *Hoxb1*$^{+/-}$ (B, H), and *Hoxb1*$^{-/-}$ (D, J) embryos. Abnormal post-otic streams of migrating NCCs (red arrowhead) are observed in *Hoxa1*$^{+/-}$;*Hoxb1*$^{+/-}$ (C, I), and *Hoxa1*$^{+/-}$;*Hoxb1*$^{-/-}$ (E, K), and *Hoxa1*$^{-/-}$;*Hoxb1*$^{-/-}$ (F, L) embryos. Asterisk indicates reduction of *Crabp1* expression in the 3rd PAA of *Hoxa1*$^{-/-}$/*Hoxb1*$^{-/-}$ (F) embryos compared to all other genotypes. ba: branchial arch; ov: otic vesicle. Scale bar: 200 μm.

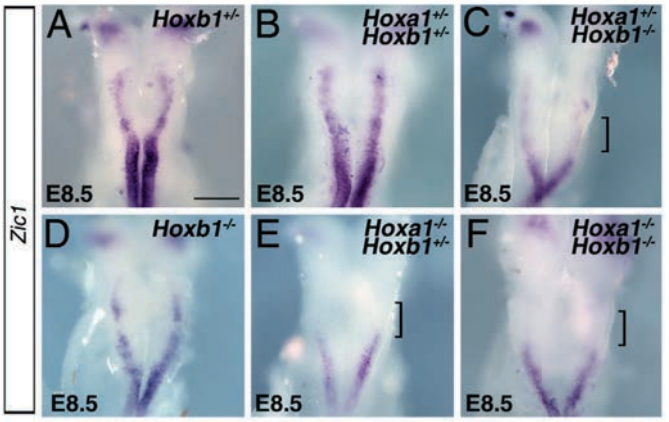

Fig. 7. *Hoxa1* and *Hoxb1* are required for neural crest specification. (A–F) Whole-mount *in situ* hybridization for *Zic1*, a marker of the neural plate border, on single and compound mutant embryos at E8.5 (7–8 s). The expression of *Zic1* in $Hoxa1^{+/-}$;$Hoxb1^{-/-}$ (C), $Hoxa1^{-/-}$;$Hoxb1^{+/-}$ (E), and $Hoxa1^{-/-}$;$Hoxb1^{-/-}$ (F) is reduced in the posterior hindbrain (brackets) compared to $Hoxb1^{+/-}$ (A), and $Hoxb1^{-/-}$ (D) embryos. Scale bar: 200 μm.

Supplementary data to this article can be found online at http://dx.doi.org/10.1016/j.mod.2016.11.006.

Authors' Contributions

MR, NB and SZ conceived and designed the experiments. MR, BL, NE, NB and SS performed the experiments. SZ interpreted data and wrote the manuscript. All authors have read and approved the manuscript.

Acknowledgements

This work was supported by the "Association Française contre les Myopathies" (NMH-Decrypt Project), the "Agence Nationale pour la Recherche (ANR-13-BSV2-0003-01), and the "Institut National de la Santé et de la Recherche Médicale" to S.Z. M.R. received a PhD fellowships from the "Ministère de l'Enseignement Supérieur et de la Recherche" and the "Association Française contre les Myopathies" (NMH-Decrypt). B.L received postdoctoral fellowships from the "Fondation pour la Recherche Médicale" and the "Agence Nationale pour la Recherche (ANR-13-BSV2-0003-01). We are grateful to Dr. R. Kelly for his comments on the manuscript. We thank Gaëlle Odelin for her technical assistance.

References

Arenkiel, B.R., Gaufo, G.O., Capecchi, M.R., 2003. Hoxb1 neural crest preferentially form glia of the PNS. Dev. Dyn. 227, 379–386.

Aruga, J., 2004. The role of Zic genes in neural development. Mol. Cell. Neurosci. 26, 205–221.

Bertrand, N., Roux, M., Ryckebusch, L., Niederreither, K., Dolle, P., Moon, A., Capecchi, M., Zaffran, S., 2011. Hox genes define distinct progenitor sub-domains within the second heart field. Dev. Biol. 353, 266–274.

Boot, M.J., Gittenberger-De Groot, A.C., Van Iperen, L., Hierck, B.P., Poelmann, R.E., 2003. Spatiotemporally separated cardiac neural crest subpopulations that target the outflow tract septum and pharyngeal arch arteries. Anat. Rec. A Discov. Mol. Cell Evol. Biol. 275, 1009–1018.

Calmont, A., Ivins, S., Van Bueren, K.L., Papangeli, I., Kyriakopoulou, V., Andrews, W.D., Martin, J.F., Moon, A.M., Illingworth, E.A., Basson, M.A., Scambler, P.J., 2009. Tbx1 controls cardiac neural crest cell migration during arch artery development by regulating Gbx2 expression in the pharyngeal ectoderm. Development 136, 3173–3183.

Carpenter, E.M., Goddard, J.M., Chisaka, O., Manley, N.R., Capecchi, M.R., 1993. Loss of Hox-A1 (Hox-1.6) function results in the reorganization of the murine hindbrain. Development 118, 1063–1075.

Chisaka, O., Capecchi, M.R., 1991. Regionally restricted developmental defects resulting from targeted disruption of the mouse homeobox gene hox-1.5. (see comments). Nature 350, 473–479.

Forlani, S., Lawson, K.A., Deschamps, J., 2003. Acquisition of Hox codes during gastrulation and axial elongation in the mouse embryo. Development 130, 3807–3819.

Gaufo, G.O., Flodby, P., Capecchi, M.R., 2000. Hoxb1 controls effectors of sonic hedgehog and Mash1 signaling pathways. Development 127, 5343–5354.

Gavalas, A., Studer, M., Lumsden, A., Rijli, F.M., Krumlauf, R., Chambon, P., 1998. Hoxa1 and Hoxb1 synergize in patterning the hindbrain, cranial nerves and second pharyngeal arch. Development 125, 1123–1136.

Goddard, J.M., Rossel, M., Manley, N.R., Capecchi, M.R., 1996. Mice with targeted disruption of Hoxb-1 fail to form the motor nucleus of the VIIth nerve. Development 122, 3217–3228.

Graham, A., Smith, A., 2001. Patterning the pharyngeal arches. Bioessays 23, 54–61.

Hoffman, J.I., Kaplan, S., 2002. The incidence of congenital heart disease. J. Am. Coll. Cardiol. 39, 1890–1900.

Hutson, M.R., Kirby, M.L., 2007. Model systems for the study of heart development and disease cardiac neural crest and conotruncal malformations. Semin. Cell Dev. Biol. 18, 101–110.

Jain, R., Engleka, K.A., Rentschler, S.L., Manderfield, L.J., Li, L., Yuan, L., Epstein, J.A., 2011. Cardiac neural crest orchestrates remodeling and functional maturation of mouse semilunar valves. J. Clin. Invest. 121, 422–430.

Jiang, X., Choudhary, B., Merki, E., Chien, K.R., Maxson, R.E., Sucov, H.M., 2002. Normal fate and altered function of the cardiac neural crest cell lineage in retinoic acid receptor mutant embryos. Mech. Dev. 117, 115–122.

Kameda, Y., Watari-Goshima, N., Nishimaki, T., Chisaka, O., 2003. Disruption of the Hoxa3 homeobox gene results in anomalies of the carotid artery system and the arterial baroreceptors. Cell Tissue Res. 311, 343–352.

Kirby, M.L., 2007. Cardiac Development. University Press, Oxford.

Kirby, M.L., Gale, T.F., Stewart, D.E., 1983. Neural crest cells contribute to normal aorticopulmonary septation. Science 220, 1059–1061.

Kirby, M.L., Hunt, P., Wallis, K., Thorogood, P., 1997. Abnormal patterning of the aortic arch arteries does not evoke cardiac malformations. Dev. Dyn. 208, 34–47.

Kirby, M.L., Waldo, K.L., 1995. Neural crest and cardiovascular patterning. Circ. Res. 77, 211–215.

Kuhlbrodt, K., Herbarth, B., Sock, E., Hermans-Borgmeyer, I., Wegner, M., 1998. Sox10, a novel transcriptional modulator in glial cells. J. Neurosci. 18, 237–250.

Li, B., Kuriyama, S., Moreno, M., Mayor, R., 2009. The posteriorizing gene Gbx2 is a direct target of Wnt signalling and the earliest factor in neural crest induction. Development 136, 3267–3278.

Li, X., Lufkin, T., 2000. Cre recombinase expression in the floorplate, notochord and gut epithelium in transgenic embryos driven by the Hoxa-1 enhancer III. Genesis 26, 121–122.

Lindsay, E.A., Baldini, A., 2001. Recovery from arterial growth delay reduces penetrance of cardiovascular defects in mice deleted for the DiGeorge syndrome region. Hum. Mol. Genet. 10, 997–1002.

Lufkin, T., Dierich, A., LeMeur, M., Mark, M., Chambon, P., 1991. Disruption of the Hox-1.6 homeobox gene results in defects in a region corresponding to its rostral domain of expression. Cell 66, 1105–1119.

Maden, M., Horton, C., Graham, A., Leonard, L., Pizzey, J., Siegenthaler, G., Lumsden, A., Eriksson, U., 1992. Domains of cellular retinoic acid-binding protein I (CRABP I) expression in the hindbrain and neural crest of the mouse embryo. Mech. Dev. 37, 13–23.

Makki, N., Capecchi, M.R., 2012. Cardiovascular defects in a mouse model of HOXA1 syndrome. Hum. Mol. Genet. 21, 26–31.

Murphy, P., Hill, R.E., 1991. Expression of the mouse labial-like homeobox-containing genes, Hox 2.9 and Hox 1.6, during segmentation of the hindbrain. Development 111, 61–74.

Plein, A., Fantin, A., Ruhrberg, C., 2015. Neural crest cells in cardiovascular development. Curr. Top. Dev. Biol. 111, 183–200.

Porras, D., Brown, C.B., 2008. Temporal-spatial ablation of neural crest in the mouse results in cardiovascular defects. Dev. Dyn. 237, 153–162.

Rossel, M., Capecchi, M.R., 1999. Mice mutant for both Hoxa1 and Hoxb1 show extensive remodeling of the hindbrain and defects in craniofacial development. Development 126, 5027–5040.

Roux, M., Laforest, B., Capecchi, M., Bertrand, N., Zaffran, S., 2015. Hoxb1 regulates proliferation and differentiation of second heart field progenitors in pharyngeal mesoderm and genetically interacts with Hoxa1 during cardiac outflow tract development. Dev. Biol. 406, 247–258.

Ryckebusch, L., Bertrand, N., Mesbah, K., Bajolle, F., Niederreither, K., Kelly, R.G., Zaffran, S., 2010. Decreased levels of embryonic retinoic acid synthesis accelerate recovery from arterial growth delay in a mouse model of DiGeorge syndrome. Circ. Res. 106, 686–694.

Soriano, P., 1999. Generalized lacZ expression with the ROSA26 Cre reporter strain. Nat. Genet. 21, 70–71.

Soshnikova, N., Dewaele, R., Janvier, P., Krumlauf, R., Duboule, D., 2013. Duplications of hox gene clusters and the emergence of vertebrates. Dev. Biol. 378, 194–199.

Studer, M., Gavalas, A., Marshall, H., Ariza-McNaughton, L., Rijli, F.M., Chambon, P., Krumlauf, R., 1998. Genetic interactions between Hoxa1 and Hoxb1 reveal new roles in regulation of early hindbrain patterning. Development 125, 1025–1036.

Studer, M., Lumsden, A., Ariza-McNaughton, L., Bradley, A., Krumlauf, R., 1996. Altered segmental identity and abnormal migration of motor neurons in mice lacking Hoxb-1. Nature 384, 630–634.